JMEPEG (2024) 33:1229–1240
https://doi.org/10.1007/s11665-023-08053-7

1059-9495/$19.00

TECHNICAL ARTICLE

Effect of Tube Extrusion Expander Shear on Recrystallization Behavior, Texture Evolution, and Mechanical Properties of Hot Deformed Mg-3Al-1Zn Alloy

Wei Zhang, Hong-jun Hu, Hui-ling Zhang, Hui Zhao, Yang Li, and Zhongwen Ou

Submitted: 25 October 2022 / Revised: 25 January 2023 / Accepted: 10 February 2023 / Published online: 20 March 2023

In this paper, a new fabrication technique for Mg-3Al-1Zn (AZ31) magnesium alloy tube, called tube extrusion expander shear (TEES), was proposed based on the existing extruded shear (ES) technique. The finite-element modeling (FEM) was used to simulate the forming process of TEES. The electron backscattered diffraction (EBSD) was used to study the microstructures and textures evolution of AZ31 magnesium alloy during TEES process. The mechanical properties of the formed tube were tested. The results show that TEES process can effectively refine the grain size and weaken the basal texture. The hardness and plasticity of the tube processed by TEES process are significantly improved, the maximum elongation is 15%, and the hardness is 78 HV. Based on the analysis of intragranular misalignment axis (IGMA), the evolutions of twins in the TEES process were studied. It was found that twins and basal slip were the main deformation modes in the early deformation zone. With development of TEES process the twins disappear and multiple sliding systems were activated. The results show that the turning and shearing zones of TEES process are beneficial to the activation of multiple slip systems.

Keywords dynamic recrystallization, magnesium alloy, microstructure, severe plastic deformation, texture

1. Introduction

Magnesium alloy is the most rapidly developing light alloy in the twenty-first century because of its light weight, good performance and good recyclability, and it is an indispensable metal material in the development of light alloys (Ref 1-3). However, their weak plasticity and low room temperature strengths are due to their hexagonal structure, which limited their wide application in industry (Ref 4, 5). Therefore, it is of great significance for developing high-quality magnesium alloy products to deeply and comprehensively analyze the deformation mechanism of magnesium alloy (Ref 6, 7).

Severe plastic deformation (SPD) is an effective way to improve the overall mechanical properties of magnesium alloys by increasing the cumulative stress to achieve grain refinement and texture control. Using SPD to improve the plasticity of magnesium alloys has become the main research direction of scholars at home and abroad. Up to now, the major SPD technologies are equal channel angular pressing (ECAP) (Ref 8), high pressure torsion (HPT) (Ref 9), cyclic extrusion compression (CEC) (Ref 10), etc. ECAP is the most common SPD technology, and its ability to achieve grain refinement has been widely proved (Ref 8, 11, 12). Traditional ECAP process can be used to prepare tubes by matching mandrel. However, due to the uneven strain applied during ECAP, various bending limitations, such as uneven deformation properties and tube thickness, are caused. The HPT process was proposed by Greenwood et al. (Ref 13) in the 1930s. On the basis of traditional extrusion forming, torsion forming is added to make the material deform under the action of pressure and shear force. Yan et al. (Ref 14) prepared magnesium alloy tubes by cup mould with stable rotation. The experiments show that the forming loads decreases when the die or punch rotates. The moderate shear strains are also produced in HPT processes due to material distortion, which promote the rotation of grains and weakening the basal texture, thus reducing the anisotropy of the alloy. However, although the existing SPD process can significantly refine the grains, most of the processes are complex and not suitable for industrial production.

As a new plastic forming method based on SPD, extrusion-shear (ES) process has the ability to refine grains and weaken textures (Ref 15-17), and stable and uniform microstructures can be obtained by single pass deformation. However, the previous methods still have some defects. For example, when a large strain was achieved, a large extrusion pressure was still required. At the same time, the influences of ES process on microstructures evolution were not clear. A new extrusion process, tube extrusion expander shear (TEES) is introduced for AZ31 magnesium alloy tube processing in this paper, and the influences of the TEES process on the microstructures evolution of magnesium alloy have been studied. In order to explore the flow law of metal during the process of TEES process, the

Wei Zhang, Hong-jun Hu, Hui-ling Zhang, Hui Zhao, and **Yang Li**, Materials Science and Engineering College, Chongqing University of Technology, Chongqing 400050, China; and **Zhongwen Ou**, School of Chemistry and Materials, Army Service College, Chongqing 401311, China. Contact e-mails: 48516686@qq.com and hhj@cqut.edu.cn.

stress and strain of TEES and DE in forming were compared by using the finite element simulation method. Microstructures evolution of the alloys at different forming zones of TEES were systematically studied by means of optical microscope (OM) and electron back scattered diffraction (EBSD), and the mechanical properties of formed tube were characterized by microhardness and tensile test. Furthermore, the deformation modes of AZ31 magnesium alloy at different zones of the TEES process have been studied by IGMA analysis. It is expected to provide technical guidance for the preparation of high-performance magnesium alloy products by ES process in the future.

2. Experiments

2.1 TEES Process

The material of TEES process is commercial AZ31 magnesium alloy, and its main chemical composition is shown in Table 1. TEES extrusion experiment adopts multi-cylinder servo synchronous extruder with nominal force 2500 kN. The extrusion experiment die and flow diagram are shown in Fig. 1(a). In this process, the punch pushes the tube billet into the extrusion die. The extrusion die consists of TEES die, container, mandrel and punching plate, which made of H13 hot working tool steel. The preheating temperature of TEES die is 360 °C, and extrusion ratio is 9.3, and extrusion speed is 4 mm/s. The punch moves in the vertical direction, which contacts with material and applies three triaxial stresses. After the final extrusion, the samples were water cooled. The die structure of TEES process is shown in Fig. 1(b), including the details of the tube forming part as Fig. 1(c).

2.2 Microstructures Characterization and Mechanical Test

To further characterize the microstructures, the samples were cut to 20 × 15 × 5 mm. The samples were taken from the center of longitudinal section in four different zones, which include upsetting zone, turning zone, shearing zone and sizing zone. Standard metallographic procedures are used to prepare for samples, including installation, grinding and polishing. The polished samples were etched with acetic acid and picric acid solution (2 mL acetic acid + 1 g picric acid + 5 mL water + 20 mL alcohol). The textures at different zones were analyzed by EBSD. EBSD samples were polished to 1200 # by SiC sandpaper before electropolishing. The liquid nitrogen controlled the polishing liquid at about − 30 °C, and the polishing voltage was 20 V, and the current was adjusted from 0.01 to 0.05 A according to the size of the testing surface, and the polishing time was 100-150 s. Post-processing of data was performed on Channel 5 and MATLAB software.

The tensile tests for DE and TEES processed samples were carried out at 22 °C with a strain rate of 0.55 mm/min. Tension specimen were used for the tensile test, which were 30 mm in length and 6 mm ± 1.0 in width overall and 20 mm in length and 2 mm in width in parallel sections, and the cross section was 2 × 2 mm.

Table 1 The chemical contents of materials (wt.%)

Billet	Chemical composition, wt.%						
AZ31	Si	Al	Zn	Mn	Fe	Cu	Mg
	0.05	3.2	0.63	0.8	0.05	0.01	Balance

2.3 Finite Element Simulation

TEES process adds turning and shearing processes on the basis of direct extrusion, which makes the material deformation process complex. In this paper, the plastic forming simulation software Deform-3D was used to simulate and compare the TEES and DE process. The finite element model was made in UG software according to 1:1 and imported into Deform-3D simulation software. Since the forming conditions of the tubes are symmetrical, the 1/2 model is adopted to improve the efficiency. The TEES die is set as a rigid body, and tube blank is set as a plastic body, and the friction coefficient is 0.2, extrusion speed is 4 mm/s, extrusion temperature is 360 °C, and the thermal conductivity is 11 N/°C S mm^2.

3. Results

3.1 Finite Element Simulation

Figure 2 shows the results of finite element analysis of DE and TEES processes. The variation of forming loads under different processes are shown in Fig. 2(b). It can be seen from the figure that the forming loads of different processes in the upsetting zone are basically the same. After entering the turning zone, the forming loads of TEES process increase slowly or even decreases. This is because the turning zone of TEES process increases the shear force distributed along the TD direction, and also promotes the rapid flows of metal to the shearing zone, thus reducing the forming loads. When the alloy passes through the middle zone of the turning zone, the load rises sharply.

Figure 2 a shows the effective strain change of the magnesium alloy tube during the preparation process. It can be seen from the figure that in the forming process of TEES, the deformation increases with the lower pressure of the punch. In the upsetting stage and before the shearing zone, the deformation of the billet increases less. After entering the shear zone, the strain increases obviously due to the large transverse tangential stress and the interaction force of the die. Figure 2(c) shows the changes in the effective strain and the effective strain rate in the TEES formation region. As can be seen from the figure, after entering the shear zone, the strain rate increases rapidly and decreases, and the strain increases accordingly, and the maximum strain value reaches 3.9 mm/mm.

3.2 Microstructures Characterization

Figure 3 shows the metallographic analysis during different zones. In the upsetting zone (Fig. 3a), the original grains of AZ31 magnesium alloy are coarse, the fibrous tissue is obvious, and there are many twins in the microstructure after upsetting deformation. Coarse primary grains are broken under mechanical action. At the same time, dislocations are concentrated at grain boundaries and twin boundaries by sliding or climbing, and dynamic recrystallization occurs firstly at the grain boundaries and twin boundaries of the original broken grains (Ref 6, 18). Under the action of the punch, the alloy descends

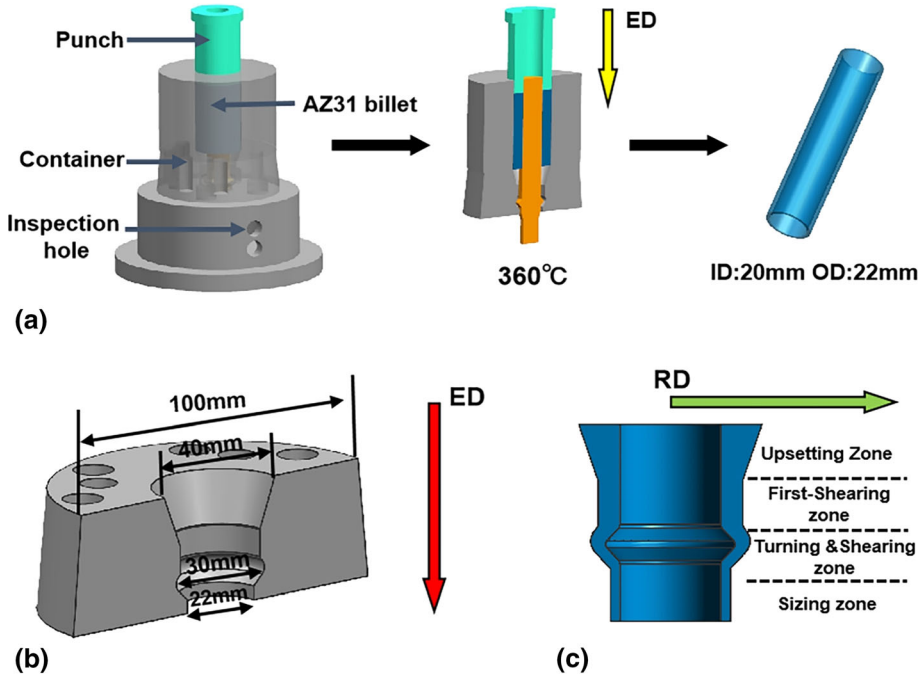

Fig. 1 (a) Diagram of TEES process (b) die structure (c) tube forming

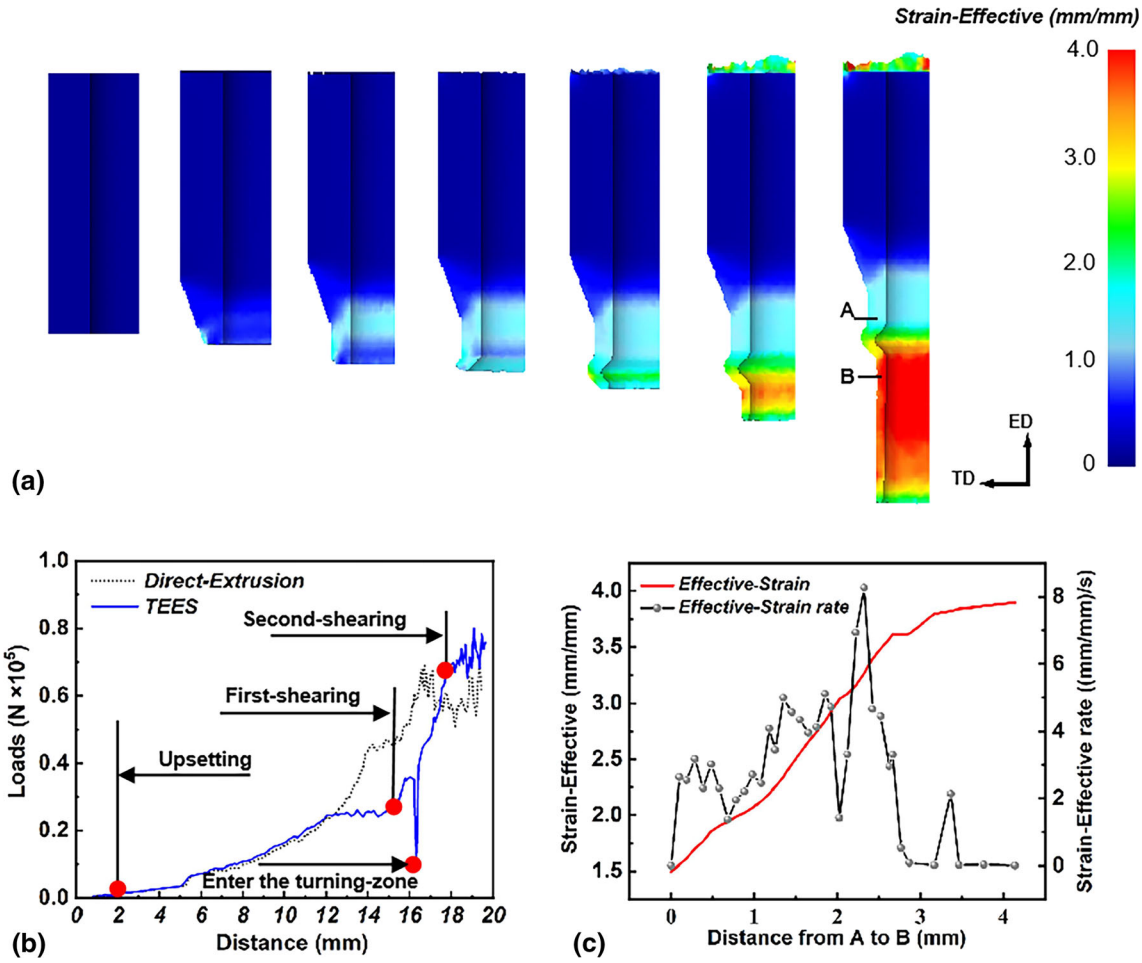

Fig. 2 FEM analysis result. (a) Effective strain cloud diagram (b) Tube forming loads (c) effective strain in TEES process

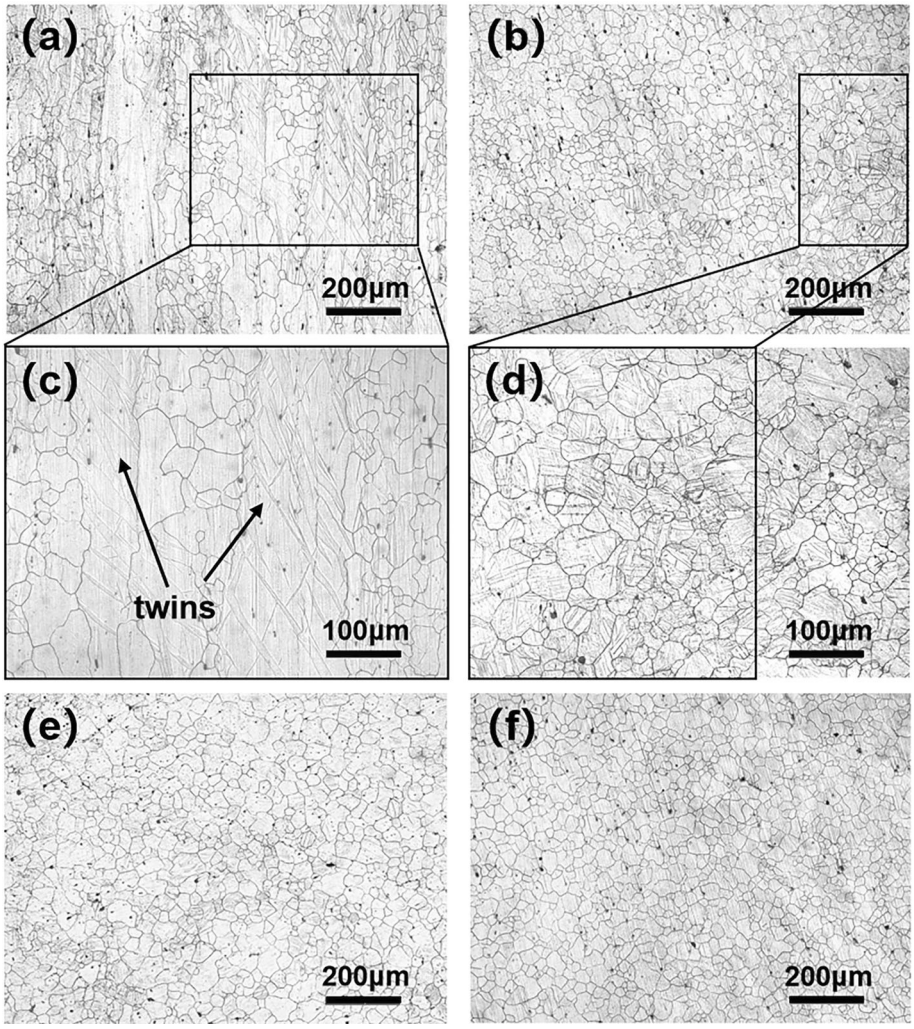

Fig. 3 Microstructures evolution during TEES process. (a), (c) Upsetting zone (b), (d) first shearing zone (e) turning & shearing zone (f) sizing zone

into the first-shearing zone, rotates relatively and redistributes among the grains due to shear stress, a certain proportion of fine and round recrystallized grains appeared in the microstructures, and appearance of some twins still visible in deformation zone (Fig. 3b, d).

From the metallographic diagram of the turning & shearing zone (Fig. 3e), it can be seen that the proportion of fine and round recrystallized grains increases significantly. Because the deformation temperature is high, and with the increase of deformation degree, the distortion energy stored in the crystal increases sharply and cannot be released in a short time, which result the nucleation number of recrystallized grains increases and dynamic recrystallization occurs further. Figure 3(f) shows the sizing zone of TEES process, there are the large number of new grains, and the average grain size is reduced to 13.89 μm. Although no longer stressed in this region, recrystallization can continue.

3.3 Microstructures Characteristics during TEES Process

In order to analyze the influences of forming mechanism on TEES process, EBSD with higher magnification is used to analyze the forming zones, so as to further illustrate the texture and grain growth of the formed zone. Figure 4(a) shows the IPF maps of four forming zones. The grain orientations change during the different zones of extrusion process, and the numbers of green and blue grains with $<$10-10$>$ and $<$11-20$>$//ED orientation increase significantly during TEES process, which indicates that the grains undergo reorientation after TEES process. In addition, obvious tensile twins can be observed in Fig. 4(a1)-(a2), which indicates twins are another important form of magnesium alloy deformation mode at the initial zone of deformation.

KAM maps for different zones of TEES process are shown in Fig. 4(b). A high KAM value indicates a high density of dislocations and the presence of local residual internal strains (Ref 6, 19, 20). The theoretical formula of strain gradient of Gao (Ref 21) and Kubin (Ref 22) shows that GNDS density is linearly related to the average KAM value.

$$\rho = \frac{2\theta^{KAM}}{ub} \qquad \text{(Eq 1)}$$

where ρ is the GND; u is the unit; b is the Burgers vector; θ^{KAM} is the average KAM value.

During the TEES process, the KAM value is maintained at a high level. Due to the high shearing stresses during the shearing zone, more moving dislocations are activated and accumulated

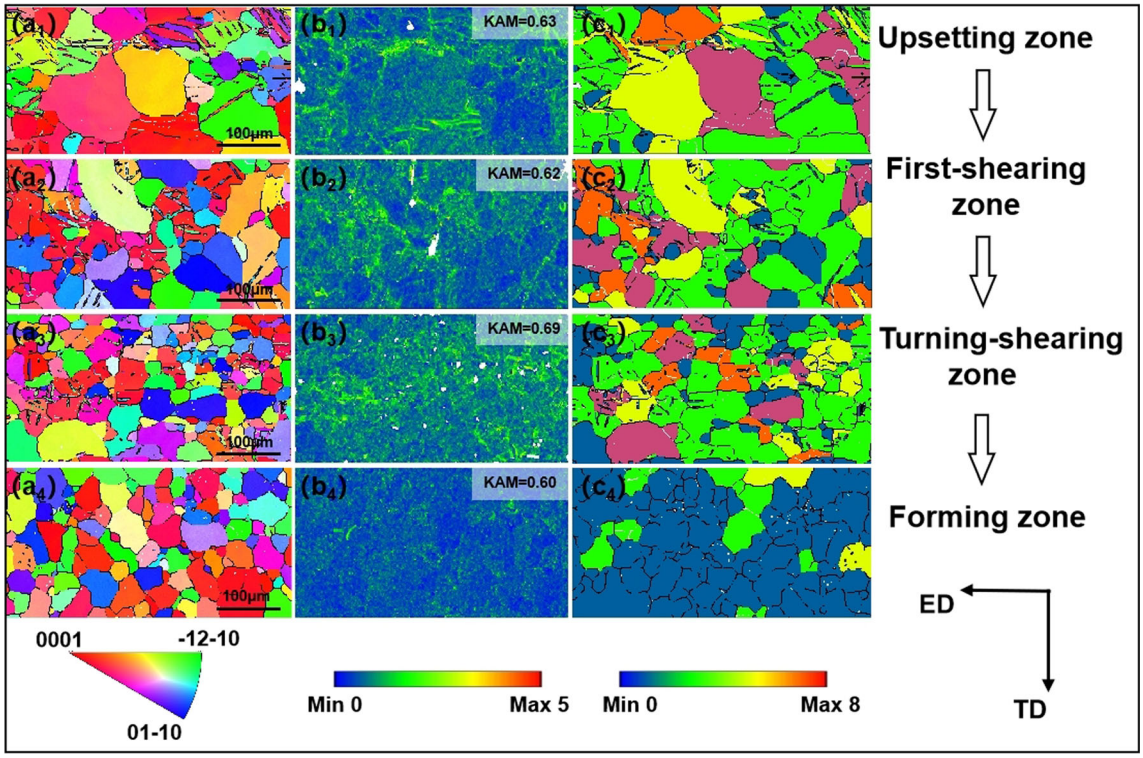

Fig. 4 Microstructure characteristics of different zones during TEES process. (a) IPF maps (b) KAM maps (c) GOS maps

in the alloy, and the KAM value increases slightly. Distortion energy difference between grains in deformed metal is the driving force of dynamic recrystallization, and recrystallization often occurs in regions with dense dislocation distribution (Ref 23). The study by Sitdikov et al. (Ref 24) reveals the process of discontinuous dynamic recrystallization (DDRX): (1) the strain imbalance in the high dislocation density region leads to the local migration of grain boundary (GB) and protrusion; (2) GB sliding occurs on the non-planar boundary, resulting in a strong strain gradient near the boundary. These dislocation sources transfer non-basal slip dislocations into grains to accommodate plastic deformation, and the high activity of non-basal slip dislocations ensures the DRX process at the later stage of TEES process. On the other hand, there are also the important reason for the decrease of twins after turning and shearing zones.

The dynamic recrystallization is usually carried out during thermal deformation. In the TEES deformation process, turning and shearing zones can increase the actual strain value, which provide sufficient deformation activation energy for dynamic recrystallization, and promote the dynamic recrystallization. The recrystallized grains are usually equiaxed, and the dislocation density inside the grains is low (Ref 23, 24). With development of TEES process, the grain sizes are refined, the strength of KAM value is reduced and the crystallization rates are increased. The recrystallization process can still be observed in the sizing zones. Therefore, we use grain orientation spread (GOS) to confirm the above description. The DRX process of magnesium alloy during hot deformation can be studied by the GOS method proposed by Hadadzadeh (Ref 25). The GOS is sensitive to the state of grains during thermal deformation. The ratio of recrystallized grains can be determined by judging the GOS value in deformed grains. According to the method in References (Ref 26, 27), grains with GOS value less than 2° were classified as recrystallized grains, and grains with GOS value more than 2° were classified as deformed grains. Figure 4(c) shows the GOS distribution at different zones. With the TEES process, the proportion of grains less than 2° increases, and the recrystallization rate increases. It can be seen from Fig. 4(c4) that most grains in the sizing area are blue or green, namely recrystallized grains. The decrease of GOS value indicates that the dislocation accumulation is low, and the dynamic recovery is good.

3.4 Texture Evolution during TEES Process

Figure 5 shows the evolutions of texture in different forming zones. In the upsetting zone, the typical basal texture appears, and the basal textures of the grains are parallel to the extrusion direction. As the tube enters the shearing zone, the temperatures of shearing zones increase under the action of continuous shearing forces, slip system becomes more active. The grains were deflected axially and laterally, and the grain orientations were deflected from $<0001>$ to the $<11\text{-}20>$ direction, and the intensities of the basal texture was also reduced from 27.97 to 16.46. Deformation and frictional heat can cause the temperature of the die exit to rise faster than that of the TEES process, resulting in static recrystallization and massive grain development after the tube leaves the extrusion die (Ref 20, 21). The {0001} pole density in the final formed sample is 10.32. After TEES process, the texture type changed and the strength decreased significantly. The c-axis of most grains of the final formed samples are about 45° with the extrusion direction, that grain orientation is conducive to the activation of the basal slip system during tensile along the extrusion direction, and improves the plastic deformation ability of the tube (Ref 26).

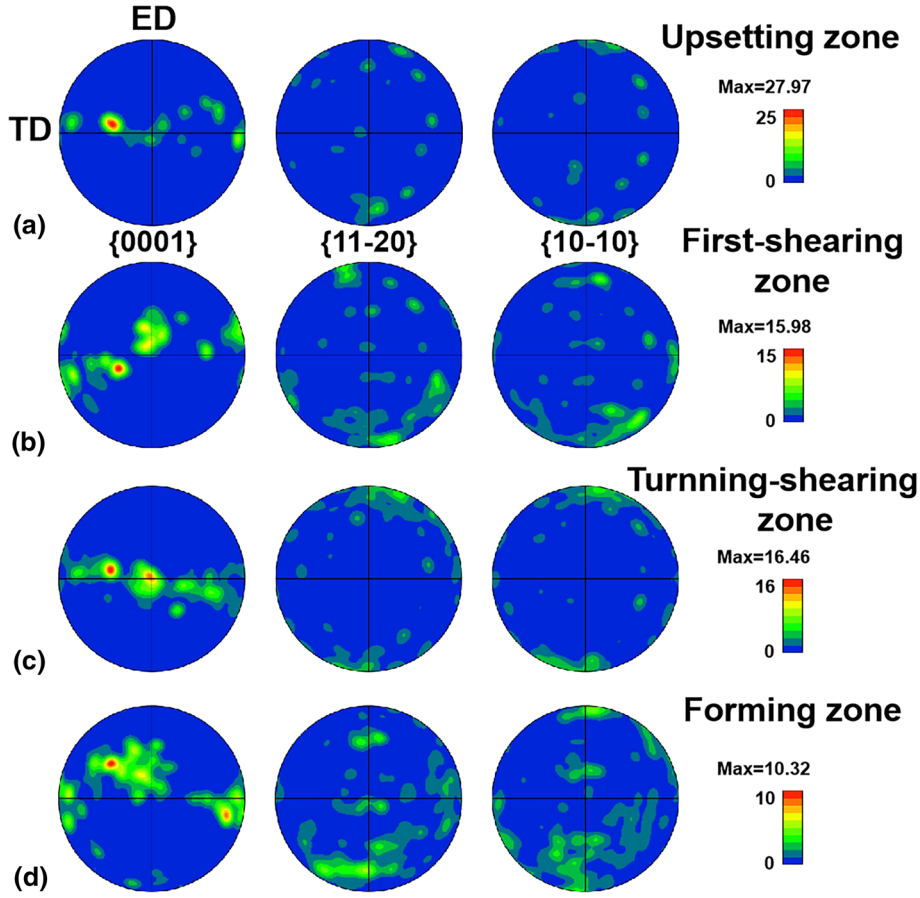

Fig. 5 Texture evolution in different forming zones. (a) Upsetting zone (b) first shearing zone (c) turning & shearing zone (d) sizing zone

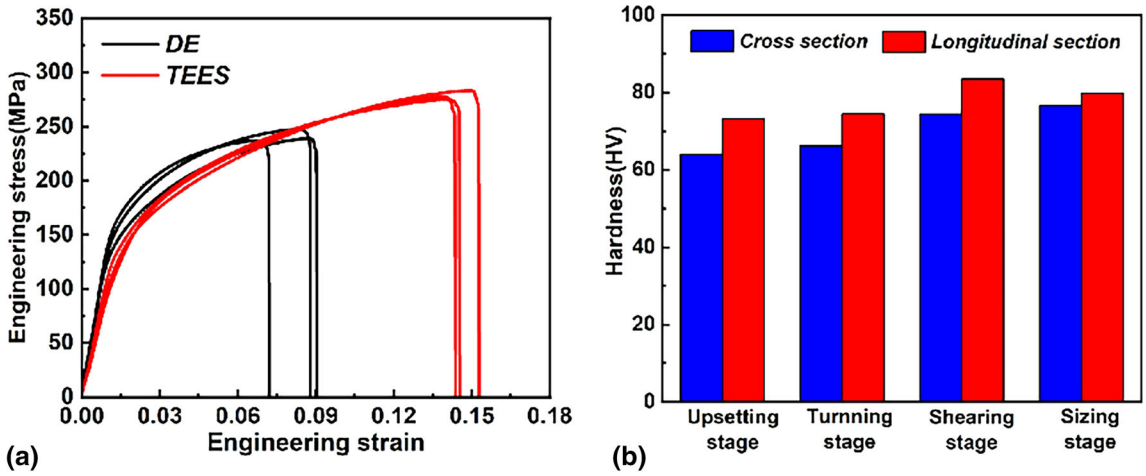

Fig. 6 Mechanical properties analysis results. (a) TEES process tensile properties compared to DE process, (b) hardness distribution at different zones of TEES process

3.5 Mechanical Properties Tests

The tensile property is an important index to measure mechanical properties of metal materials. In this section, the tensile properties of tubes prepared by different forming processes (DE and TEES process) were tested. Figure 6(a) shows the stress–strain curves. Compared with DE process, the introduction of TEES process can significantly improve the mechanical properties of formed tubes. The tensile strength of DE processed samples are 240 MPa, while that of TEES processed samples is about 280 MPa. It is worth noting that the yield strength of TEES sample is lower than that of DE process, and the yield strength of the material is often associated with the Hall–Petch formula, and grain refinement would lead to the improvement of the strength of magnesium alloy. However,

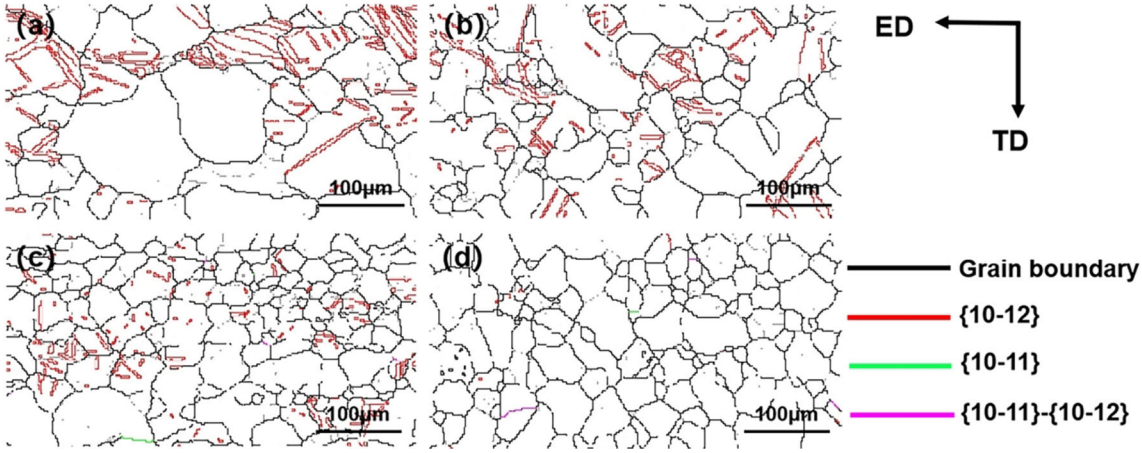

Fig. 7 Twin distributions of TEES at different zones. (a) Upsetting zone (b) first shearing zone (c) turning & shearing zone (d) sizing zone

according to Chen (Ref 28), the macroscopic mechanical properties of polycrystalline magnesium alloys do not just follow the Hall-Page formula, because the mechanical properties of polycrystalline materials are affected by grain sizes and crystal textures. For example, it can be achieved that the c-axis and extrusion direction of most grains of the final formed tube about 45° in the texture of TEES processed sample. Therefore, when stretching along the extrusion direction, {0001} base slip system Schmidt factor (SF) is larger, which is conducive to the initiation of base slip system, thus reducing the yield strength, that is, texture softening.

The TEES process includes continuous extrusion-shearing, and the work hardening and dynamic recrystallization caused by the TEES process have important influences on the hardness of the material. The effects of average grain sizes on hardness are shown in Eq. (2).

$$H_v = H_0 + kd^{-1/2} \quad \text{(Eq 2)}$$

where H_v is the room temperature hardness, d is the average grain size, H_0 is the average hardness of different positions of the AZ31 magnesium alloy tubes, and k is the strengthening coefficient.

The hardness tests were conducted on the cross section and longitudinal section of AZ31 tube at different forming zones. It can be seen from Fig. 6(b) that the hardness of the TEES processed tube is significantly improved, and the microstructures of the tube for the upsetting zone are coarse, which showing poor mechanical properties. After shearing deformation, the internal structure of the tube is more dense and the grains are refined obviously, which improves the hardness. The hardness of the shearing zone is up to 83 HV, and the hardness of the formed tube is 78 HV. From the FEM results, the hardness distribution and strain distribution of tube in TEES extrusion process are very consistent.

4. Discussion

4.1 Microstructure and Texture Evolution

Due to the lack of sufficient slip system, twinning become additional mechanisms for rapidly introducing large disorientation and accelerating the formation of new fine grains in the substructure. The twin types of magnesium alloy are mainly divided into {10-12} extension twin, {10-11} contraction twin and {10-11}-{10-12} secondary twin. The most common theory is that the twin boundary will hinder the movement of dislocation, because the twin boundary cuts off the original continuous slip system, so that the dislocation needs to constantly change the slip system, that increasing the difficulty of dislocation movement. The studies have further shown that twin dislocations are released when dislocations pass through twin boundaries, resulting in the growth or disappearance of twin lamellae. When dislocations interact with nonconforming twin boundaries, the migration ability of nonconforming twin boundaries around this point is reduced (Ref 29, 30).

Figure 7(a), (b), (c) and (d) shows the evolution of twins during TEES process. {10-12} extension twin boundaries are represented by red lines. {10-11} contraction twin boundaries are represented by green lines, and {10-11}-{10-12} secondary twin boundaries are represented by purple lines. The twin type of magnesium alloy is closely related to the load direction. In the initial zone of extrusion, {10-12} twins are inevitable under complex stress conditions due to the low critical shear stress (CRSS). In the upsetting zone, the extrusion force increases continuously, and the proportion of extension twin increases obviously under considerable extrusion pressure. The extension twins are parallel to each other in grains, forming twin boundary effectively divides and refines grains. Meanwhile, some {10-11} contraction twins are activated in the shearing zone owing to the high CRSS caused by the die corner. In fact, the C-axis of {10-11} twins tends to shrink during early zones of extrusion, but the CRSS of {10-11} contraction twins is much higher than that of {10-12} extension twins. Therefore, contraction twins are less activated in the initial extrusion.

It can be seen from Fig. 7(c) that compared with the shearing zone, tensile twins of {10-12} are significantly reduced, and the integral number of twin crystals decreases from 20.5% in the upsetting zone to 3.7%. Due to the coherent structure of {10-12} twins, their are very easy to move under continuous thermal stimulation under continuous deformation and corner friction in the shearing zone, and the subsequent CDRX process was indirectly promoted by the consumption and reorientation of the mother particles (Ref 17, 31). Figure 7(d) shows that extension twins have disappeared with

only 0.4%. The deformation twins are formed during TEES extrusion begin to degenerate and disappear during the later zone. According to Yang (Ref 32), the degradation and disappearance of twins can be explained by two reasons: (1) adjacent subgrains gradually annex deformation twins by bulge mechanism; (2) twinning laths gradually reduce the number of half bars by merging mechanism, and the half bars are widened. Finally, the twin interface of the wide strip disappears owing to the movement of dislocations.

It is worth noting that {10-11}-{10-12} secondary twins growths can be found with the extrusion process (Table 2). The growth of {10-11}-{10-12} secondary twins are related to CDRX, which indicates that dynamic recrystallization behavior is continuously activated with the TEES process (Ref 33).

4.2 Prismatic <a> Slip Activation and Lattice Rotation

In order to further explore the deformation mechanism of TEES process, the deformation modes of AZ31 alloy at different zones in TEES were analyzed by IGMA in this section. Slip and twinning are the primary deformation mechanisms of magnesium alloy. Activating more slip systems is part of the effective methods to improve the elongation properties of magnesium alloy. The slip system in Mg alloy is mainly the basal slip and non- basal slip on the {0001} basal plane, such as the {10-11} prism surface and the {10-11}, {11-22} cone surface. The starting ability of each slip system is dominated by its CRSS, and the corresponding slip is determined by the dislocation characteristics of the slip surface. Magnesium alloy can operate three basal slip systems with low CRSS values at room temperature. In contrast, high CRSS value of non- basal slip system limits the activation of non-basal slip (Ref 34). In general, resolved shear stress depends on the Schmidt factor (SF), and the SF is the orientation relationship between the sliding direction of the sliding surface and the external force, as shown below:

$$\sigma_{RSS}=\sigma_{APP} \times m \quad \text{(Eq 3)}$$

$$m = cos\lambda \times cos\phi \quad \text{(Eq 4)}$$

where σ_{RSS} is resolved shear stress, m is the Schmidt factor (SF), σ_{APP} is the applied stress, λ and ϕ are the angles between the flow stress and the sliding direction and the normal direction of the sliding surface, respectively.

When the critical shear stress of the corresponding slip system is greater than of CRSS, the corresponding slip system can be activated. When the basal and non-basal slip systems show high SF values, it indicates that they are easily activated during deformation (Ref 35). Figure 8 shows the SF of different forming zones, and the SF value is summarized in Table 3. It can be noted from the figure that the SF values of {10-10} prismatic surface are always higher than that of {0001} basal plane slip at different zones of TEES process. In addition, prismatic surfaces {10-11} also exhibit abnormal activity with an average of 0.45. At the later zone of deformation, along with

Table 2 Twin distribution at different zones

	{10-12}	{10-11}	{10-11}-{10-12}
Upsetting zone	0.230	0	0.008
First-shearing zone	0.161	0	0.024
Turning & shearing zone	0.091	0.171	0.114
Sizing zone	0.004	0.050	0.316

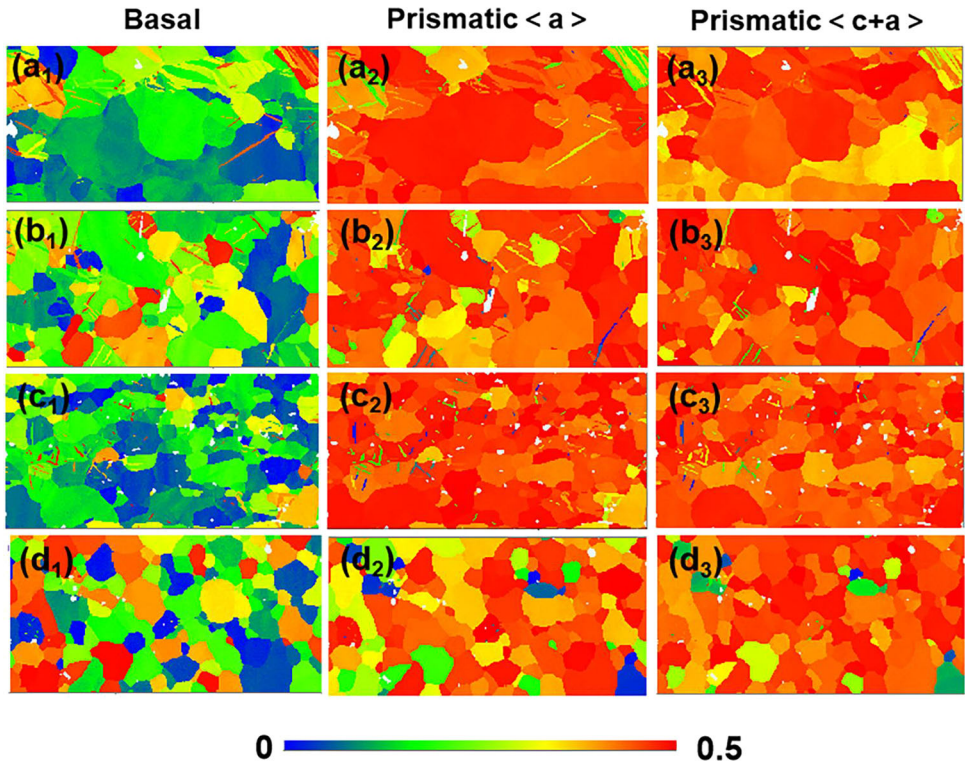

Fig. 8 Schmidt factors in different forming zones of TEES. ($a_{1\text{-}4}$) Upsetting zone ($b_{1\text{-}4}$) first shearing zone ($c_{1\text{-}4}$) turning & shearing zone ($d_{1\text{-}4}$) sizing zone

the lower stress and strain and the lower temperature at the die exit, the prismatic slip activity decreases and the SF value of the base surface increases. In general, during the TEES process, the non-base slip system is easily activated.

In order to further confirm the deformation mechanism of TEES process, the intragranular misalignment axis (IGMA) was used to confirm the initiation of different slip systems during deformation. According to the theory proposed by Chun (Ref 36, 37), the crystal will rotate around a specific crystal axis in the sliding process, and the IGMA method mainly uses this characteristic to distinguish the type of slip system, and we call this particular crystal axis Taylor axis, which can be determined by formula (6):

$$T_S = n_s \times d_s \quad \text{(Eq 6)}$$

where T_S is the Taylor axis direction, n_s and d_s are the normal and slip direction of slip surface respectively.

The corresponding table of Taylor axis and magnesium alloy sliding system determined by Formula (6) is given in Table 4. The traditional IGMA method can only discriminate the dominant slip system, because the discrimination of the dominant slip system can ignore the influence of other slip systems on the Taylor axis deflection, so it is suitable for hcp metal with less slip system. EBSD data at different forming zones were processed by Channel 5, and different grain orientation angles (0°-3°) at different forming zones were selected for plotting as shown in Fig. 9. According to the Taylor axis represented by the color band distribution of the antipolar map, the sliding system of grain initiation can be judged. It is well known that the IGMA around the direction may be caused by basal slip and conical slip, and the IGMA mainly located nearby is caused by prism slip activation. Figure 9(a) shows the distribution of grain IGMA with high schmid factor in upsetting zone. IGOS distribution of most grains is relatively uniform mainly in the <01-10> and <10-12> directions, and some grains show low strength in the <0001> direction (G5). Although the Taylor axis presented by the basal <a> and the pyramidal II <c + a> in the IGMA analysis is the same, but the CRSS of pyramidal II <c + a> slip is much higher than the basal <a>. Therefore, we can judge that the basal slip dominates the intragranular deformation at the early zone of TEES process.

Table 3 Schmidt factors at different forming zones

	Basal	Prismatic	Pyramidal
Upsetting zone	0.167	0.454	0.460
First-shearing zone	0.234	0.430	0.456
Turning & shearing zone	0.151	0.454	0.455
Sizing zone	0.260	0.382	0.427

With the TEES processing, the tube enters the shearing zone, under the action of shear force and extrusion force, the grain deflection occurs, and the texture intensity is significantly reduced, which makes the basal texture deflect to the ED direction (Fig. 4, 9bc). According to the discrete pole figure in Fig. 9c, with the deformation progress, the deformations of each grain is more complex, and the distribution of IGMA is quite different. The distribution of IGMA near the <0001> is stronger than that in the upsetting zone, which means that more cylinder slip is activated with the increase of deformation and temperature. Meanwhile, IGMA distribution of most grains is discrete (G1, G2, G4, G6), which means that multiple slip systems are jointly activated (Ref 24). In the sizing zone, further grain refinement can be noted. Distribution strength of IGMA is similar to that of the turning & shearing zone, which showing uniform distribution, but the strength reduces. Therefore, the IGMA analysis results confirmed that a variety of slip systems were activated in the later zone of TEES process.

5. Conclusion

In this paper, a new type of magnesium alloy tube preparation technology, namely TEES, is proposed based on SPD technology, and the magnesium alloy tube is successfully prepared. The micro-evolution and deformation mechanism in TEES process were analyzed by FEM and micro-characterization, and the mechanical properties of formed tubes were tested. The results show that:

- The FEM results show that the effective strain distribution in the shear deformation zone is uniform during the TEES process, and the final effective strain accumulation value is about 1.5 times higher than DE process.
- The grain refinement effect is obvious in the TEES process, and the grains in the final formed tube are about 13.89 μm. The microhardness test showed that the plasticity and the hardness of the tubes are significantly improved after TEES process, and the hardness of the formed tube is about 78 HV, and the maximum elongation is about 15%.
- During the TEES process, the texture strength and type changed significantly, and strength of basal texture decreased from 30.30 to 10.33. Most of the c-axis of grain in the microstructures of formed tube was 45° relative to the extrusion direction, which is beneficial to improve the plastic deformation ability of the tube.
- The analysis of IPF, SF and IGMA shows that the plastic deformation of AZ31 magnesium alloy is mainly regulated by slip and twin during TEES process. In the initial zone of deformation, twin and basal slip becomes the main

Table 4 Taylor axis direction of four kinds of magnesium and magnesium alloy sliding system

Slip mode	Slip type	Burgers vector	Slip system	Taylor axes
{0001}<11-20>	Basal	a/3<11-20>	3	< 1-100>
{10-10}<1-210>	Prismatic<a>	a/3<11-20>	3	<0001>
{10-11}<1-210>	Pyramidal<a>	a/3<11-20>	6	<10-12>
{10-11}<11-2-3>	Pyramidal I <c + a>	a/3<11-2-3>	12	<-2-541-1-69>
{11-22}<11-2-3>	Pyramidal II <c + a>	a/3<11-2-3>	6	<-1100>

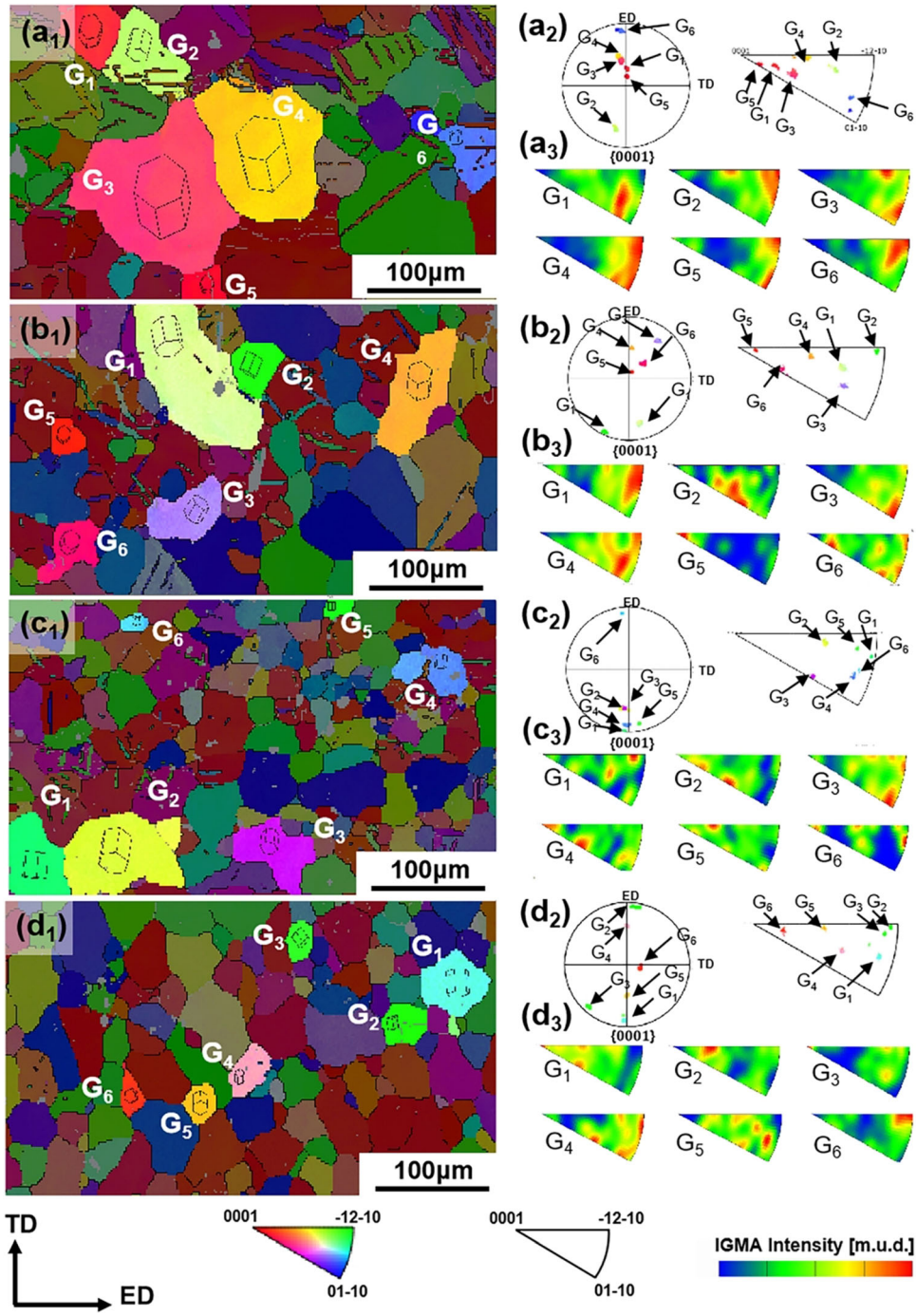

Fig. 9 IGMA analysis at different forming zones. (a) Upsetting zone (b) first shearing zone (c) turning & shearing zone (d) sizing zone

deformation mode due to the low CRSS, resulting in grain refinement. When the deformation reaches the later zone, the twins disappear basically, and the multiple slip systems dominate the deformation.

Acknowledgments

This work was supported by Chongqing Talent Plan (CQYC202003047), and Chongqing Natural Science Foundation project of cstc2018jcyjAX0653).

Authors' contributions

WZ done the experiments in this paper. HH is the corresponding author of this paper who wrote the paper. HZ done the simulation in this paper. HZ done the testings in this paper. YL done the testings in this paper. ZO the second corresponding author in this paper.

Data Availability

The raw/processed data required to reproduce these findings cannot be shared at this time as the data also forms part of an ongoing study.

Conflict of interest

The authors declare that they have no competing interests.

Ethical Approval

No animals have been used in any experiments.

Consent to Participate

There are no human who have been used in any experiments.

Consent for Publication

The authors confirm that the work described has not been published before (except in the form of an abstract or as part of a published lecture, review, or thesis); that it is not under consideration for publication elsewhere; that its publication has been approved by all co-authors, if any; and that its publication has been approved (tacitly or explicitly) by the responsible authorities at the institution where the work is carried out. The authors agree to publication in the journal indicated below and also to publication of the article in English by Springer in Springer's corresponding English-language journal.

References

1. P. He, Development and Application of Lightweight High-strength Metal Materials, *MATEC Web Conf.*, 2018, **207**(6), p 03010. https://doi.org/10.1051/matecconf/201820703010
2. I.J. Polmear, Magnesium Alloys and Applications, *Met. Sci. J.*, 1994, **10**(1), p 1–16. https://doi.org/10.1179/mst.1994.10.1.1
3. J. Yang, Y. Xu, and X. He, *Research Progress of Magnesium and Magnesium Alloys Implants in Orthopedics*, J. Repar. Reconstr. Surg, Chin, 2016. https://doi.org/10.7507/1002-1892.20160321
4. Q. Liu, X. Zhou, H. Zhou et al., The Effect of Extrusion Conditions on the Properties and Textures of AZ31B Alloy, *J. Magnes. Alloys*, 2017, **5**(2), p 202–209. https://doi.org/10.1016/j.jma.2017.03.002
5. R.S. Cheng, H.C. Pan, D.S. Xie et al., Research Progress of New High-Strength Low-Alloyed Magnesium Alloys, *Adv. Mater. China*, 2020, **39**(1), p 9. https://doi.org/10.7502/j.issn.1674-3962.201909013
6. M.G. Jiang, C. Xu, H. Yan, G.H. Fan, T. Nakata, C.S. Lao, R.S. Chen, S. Kamado, E.H. Han, and B.H. Lu, Unveiling the Formation of Basal Texture Variations Based on Twinning and Dynamic Recrystallization in AZ31 Magnesium Alloy During Extrusion, *Acta Mater.*, 2018, **157**, p 53–71. https://doi.org/10.1016/j.actamat.2018.07.014
7. X. Chen, D. Xia, J. Zhang, G. Huang, K. Liu, A. Tang, B. Jiang, and F. Pan, Ultrafine-Grained Al-Zn-Mg-Cu Alloy Processed via Cross Accumulative Extrusion Bonding and Subsequent Aging: Microstructure and Mechanical Properties, *J. Alloys Compd.*, 2020, **846**, p 156306
8. C.F. Davis, A.J. Griebel, and T.C. Lowe, Isothermal Continuous Equal Channel Angular Pressing of Magnesium Alloy AZ31, *JOM J. Miner. Met. Mater. Soc.*, 2020, **72**(7), p 2603–2611
9. N.R. Overman, S.A. Whalen, M.E. Bowden, M.J. Olszta, K. Kruska, T. Clark, E.L. Stevens, J.T. Darsell, V.V. Joshi, X. Jiang, K.F. Mattlin, and S.N. Mathaudhu, Homogenization and Texture Development in Rapidly Solidified AZ91E Consolidated by Shear Assisted Processing and Extrusion (ShAPE), *Mater. Sci. Eng. A*, 2017, **701**, p 56–68. https://doi.org/10.1016/j.msea.2017.06.062
10. X. Xian-Ming, X. Rui, X. Ke-Min et al., Effect of Cyclic Extrusion and Compression on Microstructure and Mechanical Properties of Extruded ZK60 Magnesium Alloy, *J. Plast. Eng.*, 2017, **24**(3), p 78–83
11. L.B. Tong, J.H. Chu, W.T. Sun, Z.H. Jiang, D.N. Zou, S.F. Liu, S. Kamado, and M.Y. Zheng, Development of a High-Strength Mg Alloy with Superior Ductility Through a Unique Texture Modification from Equal Channel Angular Pressing, *J. Magnes. Alloys*, 2021, **9**(3), p 1007–1018. https://doi.org/10.1016/j.jma.2020.03.011
12. H. Huang, H. Liu, C. Wang, J. Sun, J. Bai, F. Xue, J. Jiang, and A. Ma, Potential of Multi-pass ECAP on Improving the Mechanical Properties of a High-Calcium-Content Mg-Al-Ca-Mn Alloy, *J. Magnes. Alloys*, 2019, **7**(4), p 617–627. https://doi.org/10.1016/j.jma.2019.04.008
13. H. Greenwood and F.C. Thompson, Wires Drawn Through Rotating Dies, *Nature*, 1931, **128**(3221), p 152–152
14. L. Yan, Z. Zhang, Y. Xue, J. Xu, B. Dong, and X. Li, Effect of Rotating Shear Extrusion on the Microstructure, Texture Evolution and Mechanical Properties of Mg-Gd-Y-Zn-Zr Alloy, *J. Alloys Compd.*, 2022, **906**, p 164406. https://doi.org/10.1016/j.jallcom.2022.164406
15. D. Zhang, H. Hu, F. Pan, M. Yang, and J. Zhang, Numerical and Physical Simulation of New SPD Method Combining Extrusion and Equal Channel Angular Pressing for AZ31 Magnesium Alloy, *Trans. Nonferrous Met. Soc. China*, 2010, **20**(3), p 478–483. https://doi.org/10.1016/S1003-6326(09)60165-5
16. H. Hongjun, Q. Xi, Z. Dingfei et al., A Novel Severe Plastic Deformation Method for Manufacturing AZ31 Magnesium Alloy Tube, *Int. J. Adv. Manuf. Technol.*, 2018, **98**, p 897–903
17. Y. Tian, H. Hu, H. Zhao, W. Zhang, C. Liang, B. Jiang, and F. Zhang, A Novel Extrusion-Shear-Expanding Process for Manufacturing AZ31 Magnesium Alloy Tube, *Trans. Nonferrous Met. Soc. China*, 2020, **32**, p 2569–2577
18. W. Huang, J. Chen, R. Zhang, X. Yang, L. Jiang, Z. Xiao, and Y. Liu, Effect of Deformation Modes on Continuous Dynamic Recrystallization of Extruded AZ31 Mg Alloy, *J. Alloys Compd.*, 2022, **897**, p 163086. https://doi.org/10.1016/j.jallcom.2021.163086
19. T. Zhou, Q. Zhang, Q. Li, L. Wang, Q. Li, and D. Liu, A Simultaneous Enhancement of Both Strength and Ductility by a Novel Differential-Thermal ECAP Process in Mg-Sn-Zn-Zr Alloy, *J. Alloys Compd.*, 2021, **889**, p 161653. https://doi.org/10.1016/j.jallcom.2021.161653
20. S.W. Lee, S.-H. Kim, W.-K. Jo, W.-H. Hong, W. Kim, B.G. Moon, and S.H. Park, Twinning and Slip Behaviors and Microstructural Evolutions of Extruded Mg-1Gd Alloy with Rare-Earth Texture During Tensile Deformation, *J. Alloys Compd.*, 2019, **791**, p 700–710. https://doi.org/10.1016/j.jallcom.2019.03.316
21. C.S. Han, H. Gao, Y. Huang et al., Mechanism-Based Strain Gradient Plasticity: I. Theory, *J. Mech. Phys. Solids*, 1999, **47**(5), p 1239–1263
22. L.P. Kubin and A. Mortensen, Geometrically Necessary Dislocations and Strain-Gradient Plasticity: A Few Critical Issues, *Scr. Mater.*, 2003, **48**(2), p 119–125. https://doi.org/10.1016/S1359-6462(02)00335-4
23. T. Al-Samman and G. Gottstein, Dynamic Recrystallization During High Temperature Deformation of Magnesium, *Mater. Sci. Eng. A*, 2008, **490**(1–2), p 411–420. https://doi.org/10.1016/j.msea.2008.02.004
24. O. Sitdikov and R. Kaibyshev, Dynamic Recrystallization in Pure Magnesium, *Mater. Trans.*, 2005, **42**(9), p 1928–1937
25. A. Hadadzadeh, F. Mokdad, M.A. Wells, and D.L. Chen, A New Grain Orientation Spread Approach to Analyze the Dynamic Recrystallization Behavior of a Cast-Homogenized Mg-Zn-Zr Alloy Using Electron Backscattered Diffraction, *Mater. Sci. Eng. A*, 2018, **709**, p 285–289. https://doi.org/10.1016/j.msea.2017.10.062
26. S.I. Ghazanlou, B. Eghbali, and R. Petrov, Microstructural Evolution and Strengthening Mechanisms in Al7075/ Graphene Nano-plates/ Carbon Nano-tubes Composite Processed Through Accumulative Roll Bonding, *Mater. Sci. Eng. A*, 2021, **807**, p 140877. https://doi.org/10.1016/j.msea.2021.140877
27. L. Ouyang, Y. Gui, Q. Li, and Y. Fan, Isothermal Compression Bonding Mechanism and Mechanical Properties of WE43 Magnesium-Rare Earth Alloy, *Mater. Sci. Eng. A*, 2021, **822**, p 141664. https://doi.org/10.1016/j.msea.2021.141664
28. Z. Chen, W. Xia, Y. Chen, and D. Fu, Texture and Anisotropy in Magnesium Alloys, *Trans. Nonferrous Met. Soc. China*, 2005, **15**(1), p 11
29. S.G. Hong, S.H. Park, and S.L. Chong, Role of {10–12} Twinning Characteristics in the Deformation Behavior of a Polycrystalline Magnesium Alloy, *Acta Mater.*, 2010, **58**(18), p 5873–5885
30. Z. Zhang, Twinning Related Plastic Mechanism of a Magnesium Alloy at a High Strain Zone of Ambient Sheath Extrusion, *Mater. Lett.*, 2014, **119**, p 79–83. https://doi.org/10.1016/j.matlet.2013.12.098
31. X. Hu, L. Chai, Y. Zhu, H. Wu, J. Luo, L. Tian, Q. Sun, Y. Li, and J. Cheng, Quantitative Study of Microstructural, Textural and Hardness Evolution of High-Purity Ti Sheet During Rolling from Low to Medium Strains, *Mater. Today Commun.*, 2021, **29**, p 102989. https://doi.org/10.1016/j.mtcomm.2021.102989
32. G. Yang, J.-l Sun, N.-l Zhang et al., Annihilation of Deformation Twins and Formation of Annealing Twins, *J. Iron Steel Res.*, 2009, **21**(2), p 5
33. Z. Wang, G. Cao, F. Wang, L. Zhou, P. Mao, X. Jiang, and Z. Liu, Investigation of the Microstructure and Properties of Extrusion-Shear

Deformed ZC61 Magnesium Alloy Under High Strain Rate Deformation, *Mater. Charact.*, 2021, **172**, p 110839. https://doi.org/10.1016/j.matchar.2020.110839

34. H.-S. Jang, J.-K. Lee, A.J.S.F. Tapia, N.J. Kim, and B.-J. Lee, Activation of Non-basal $<c + a>$ Slip in Multicomponent Mg Alloys, *J. Magnes. Alloys*, 2022, **10**(2), p 585–597. https://doi.org/10.1016/j.jma.2021.03.007
35. S.-H. Zhang, S.-G. Song, Xu. Yong et al., Application of Schmid Factor in Mg Alloy Deformation Micro-mechanism Investigation, *J. Netshaper Form. Eng.*, 2014, **6**(6), p 7
36. Y.B. Chun, M. Battaini, C.H.J. Davies et al., Distribution Characteristics of In-Grain Misorientation Axes in Cold-Rolled Commercially Pure Titanium and Their Correlation with Active Slip Modes, *Metall. Mater. Trans. A.*, 2010, **41**(13), p 3473–3487
37. Y.B. Chun and C.H.J. Davies, *The Evolution of In-Grain Misorientation Axes (IGMA) During Deformation of Wrought Magnesium Alloy AZ31*, Springer, Berlin, 2016